Review Article

Effect of β-Fe Precipitates on the Mechanical Behavior of Al-Si Alloys with Critical Fe, Inoculated via Nb+B and Precipitation Hardened
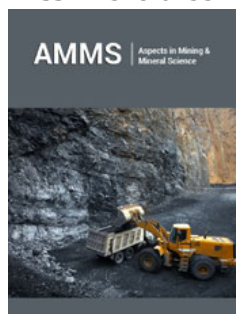
Carlos Narducci Junior[1,2,3]* and Antonio Jorge Abdalla[3]

[1]Federal Institute of São Paulo, IFSP Itaquaquecetuba, Brazil

[2]Aeronautics Institute of Technology, ITA São José dos Campos, Brazil

[3]Institute for Advanced Studies, IEAv São José dos Campos, Brazil

*Corresponding author: Carlos Narducci Junior, Rua Alto Garças, Cidade Patriarca, São Paulo-SP, Brazil

Abstract

The challenge of this research is to produce safety parts in Al-Si alloys with Fe-critical. The innovation is in studying the morphology of β-Fe and Mg_2Si precipitates in the mechanical behavior of the material after the addition of NbB and the heat treatment. Aiming to improve the mechanical properties of AlSi alloys coming from recycling (Fe-critical) by manipulating the β-Fe precipitates and maintaining the Mg_2Si precipitates. The samples were cast with Al10Si1Fe0.35Mg alloy, inoculated via NbB, and pouring in a metal mold according to ASTM B108. The microstructure was analyzed with BSE-SEM and EDS. The work investigated the morphology of β-Fe precipitates and their effects and interactions on the material's mechanical properties. The combined effect of the addition of NbB and Mg elements, with subsequent artificial aging of the material, resulted in the reduction and spheroidization of the β-Fe precipitates, providing higher proof strength (YS=207.71MPa), Ultimate Tensile Strength (UTS=300.35MPa) and elongation of 4.66 %.

Keywords: Recycled Al-Si alloys; Nb+B; Casting; Heat treatment; Mechanical properties; Grain refinement; Intermetallic precipitates

Introduction

The iron element (Fe) in aluminum alloys is a subject widely discussed in various research and consolidated as being harmful to the material's mechanical properties, such as tensile strength, fatigue, fracture toughness, and, mainly, the ductility of the material. During the solidification occurs the formation of the intermetallic phase $β-Al_5FeSi$ (β-Fe), with thick morphology in the form of plate or needle, it becomes rigid points in the soft structure of the material that, when subjected to stresses, initiate small cracks that extend into fissures that eventually decrease its mechanical properties [1-6]. Current studies show that the inoculation of the material by adding NbB caused an exponential increase of nucleation points (heterogeneous nucleation), forming a large number of simultaneous grains that ended up restricting the mobility of the solute elements and thus decreasing their interconnectivity and also the formation of agglomerates and finally presenting a refined grain structure with reduced and spheroidized β-Fe intermetallic precipitates [7-11]. Figure 1 is a schematic representation illustrating how the mechanism of modification occurs. This study used the beneficial action of heterogeneous nucleation in modifying the morphology of second phase precipitates, as shown in Figure 1, adding simultaneously with the precipitation hardening technique by an alloying element (Mg) to the material, with subsequent solubilization and precipitation (heat treatment-T6), to allow finely dispersed particles of the supersaturated solid solution [12], aiming for an improvement in its mechanical properties. The summary, as shown in (Figure 2), is one way of presenting the hypothesis in question.
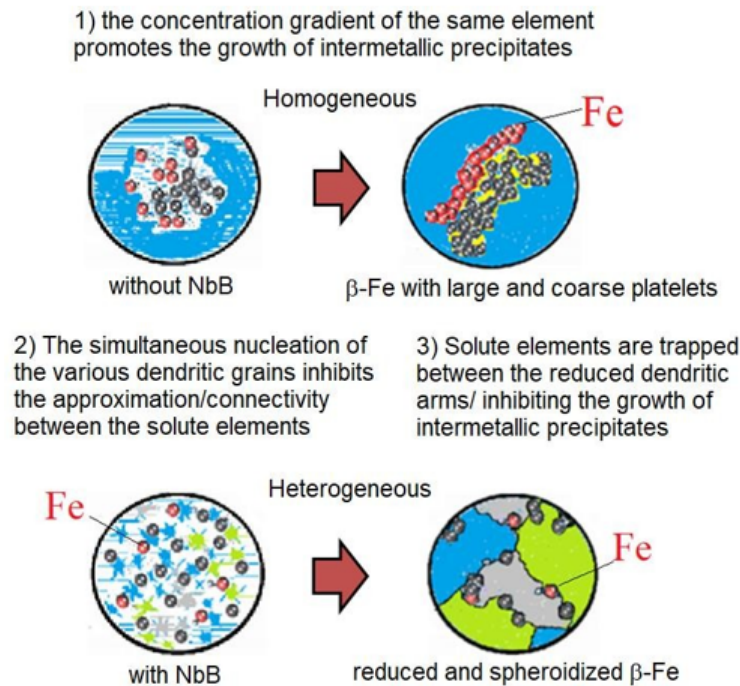
1) the concentration gradient of the same element promotes the growth of intermetallic precipitates

Homogeneous

without NbB

β-Fe with large and coarse platelets

2) The simultaneous nucleation of the various dendritic grains inhibits the approximation/connectivity between the solute elements

3) Solute elements are trapped between the reduced dendritic arms/ inhibiting the growth of intermetallic precipitates

Heterogeneous

with NbB

reduced and spheroidized β-Fe

Figure 1: Schematic representation of mechanism β-Fe modification occurs, adapted from (Narducci, 2021).

If, ∀ AlSi ⊃ (Fe-critical) ∃ β-Fe (large and coarse) ⇒ < strength ∧ < ductility (material), with the assumption of:	problem
+ NbB ⇒ {(heterogeneous nucleation | < α-Al grain size) ⇒ < β-Fe morphology | (reduced and spheroidized)}= gain > strength (material) ∧ + Mg + T6 ⇒ {Mg₂Si (coherent precipitates) ∧ β-Fe morphology | (distorted and decomposed)} = gain > ductility (material), then:	hypothesis
∑ NbB +Mg +T6 ⇒ { < β-Fe ∧ Mg₂Si} = gain > strength ∧ > ductility (material)	result

∀ for every; ⊃ contains; ∃ exists; ⇒ implies that; < minor; > greater; + addition; | such that.

Figure 2: Summary with the problem, hypothesis, and results written with mathematical expressions.

Experimental Procedure

The experimental procedure consisted of producing specimens (CDPs) for tensile testing. The CDPs were manufactured in SUNY Foundry- Itaquaquecetuba, Br. The metal was melted in an electric crucible oven, with a capacity of 60kg of material. After adding each element, the temperature was stabilized at 850±10 °C, with a 1-hour hold was applied to ensure complete dissolution. Degassing was then carried out by adding hexachloroethane tablets. For each sample collection, achieved homogenization by 30s of stirring and a new temperature stabilization at 720±10 °C, followed by a second homogenization at the same temperature, with 30s of stirring and sample collection. The casting was done in the Gravity Die Casting (GDC) process, using a 1020 steel metal mold, manufactured according to ASTM B108 (supplied by Alpha Trend). The mold was built in two halves and with two cavities (producing two CDPs per pour). The mold feeding system was made with a central filling channel that distributes the metal in two auxiliary side feeding channels, making the liquid metal feed the product from bottom to top and through two inlet channels in each part. This system minimizes material turbulence during part filling, as shown in Figure 3a). Before pouring the liquid metal, the mold was painted with water-based graphite paint and heated with a torch to 250 °C, (Figure 3b). The metal was poured into the mold by hand, with a metal spoon, until it was filled, (Figures 3c-3f). The cooling time was 3 minutes, then the mold was opened, and the CDPs were unmolded 2f). The production was of 20 CPDs for each type of material (10 pouring's). The chemical composition of each batch produced is shown in Table 1. The verification of the base alloy was done by atomic absorption spectrometry.
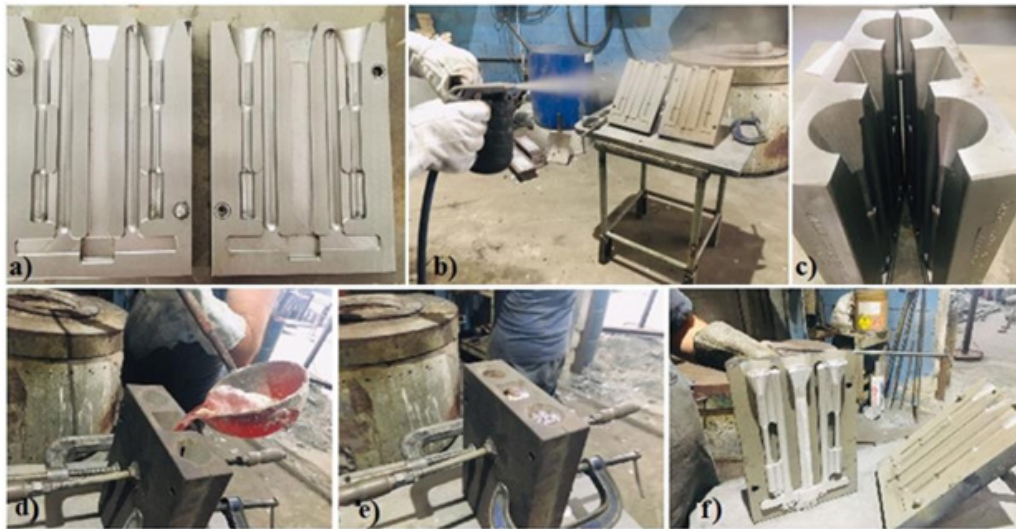
Figure 3: Gravity casting mold for production of the CDPs. a) Two halves and two cavities. b) Painting the mold. c) Closing the mold. d) Manual pouring with the spoon. e) Closed mold waiting for the material to cool. f) Open mold with the CPDs.

Table 1: Chemical composition of TTS.

Batch	Elements (Wt. %)					
	Al	Si	Fe	Nb	B	Mg
1º	balance	10	1	0	0	0
2º	balance	10	1	0,05	0,00625	0
3º	balance	10	1	0,05	0,00625	0,35
4º	balance	10	1	0	0	0,35

The heat treatment (T6) was carried out in a muffle furnace, located in the metallurgy laboratory of ITA. The T6 heat treatment parameters used were temperature of 535±5 °C, duration of 4h±15' (solubilization), transferred immediately to a water tank at room temperature (25 ºC) for 15 minutes (quenching). Then, the TTS group was heated at a temperature of 175±5 °C, duration of 7h±15' (precipitation or artificial aging), with subsequent cooling in the open air. Figure 4 shows the curve with the treatment route applied in the process for the intended specific precipitation (T6). To analyze the grain size, took the samples' cross-sectional surfaces from the central body of the TTS, cut in the horizontal and vertical directions when filling the piece, prepared with 2400 mesh sandpaper sheets without polishing. After the metallurgical preparation, attacked the samples for 15 seconds with a Poulton acid solution. For the analysis of the microstructural constituents, the cross-section surfaces, after being prepared with 2400 mesh sandpaper sheets, were polished with a 1μm alumina suspension and then chemically attacked with the Keller reagent. The macro- and microstructures were examined in an optical microscope with polarized light, filter plate, and Differential Interference Contrast (DIC). The measurement of the average grain size (G) was conducted by the linear intercept method according to the ASTM E112-10 standard, 1996. The β-Fe intermetallic precipitate was analyzed by X- ray Dispersive Energy Spectroscopy (EDS) with the aid of a Tescan scanning electron microscope from Oxford Instruments. The tensile test was performed in a universal machine (brand Quanteq),

model Emic Trd28 and equipped with a TestScript304 software for testing methods, located in the metallurgy laboratory of the Federal Institute of São Paulo (IFSP) - Campus Itaquaquecetuba. The data obtained were Yield Strength (YS), Ultimate Tensile Strength (UTS), and elongation (%). Three CDPs were tested for each batch of material according to the chemical composition detailed in Figure 2, without and with the addition of Nb+B, Mg, and subsequent heat treatment (T6), with five test conditions, as follows:
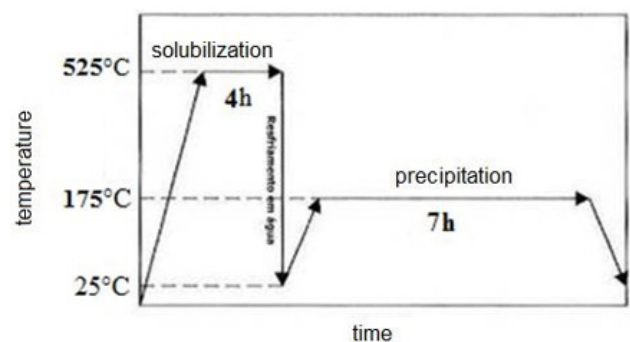

Figure 4: Solubilization treatment followed by rapid cooling and precipitation.

a. Base material;

b. Base material with added Mg and T6;

c. Base material with added Nb+B;

d. Base material with addition of Nb+B and T6;

e. Base material with added Mg, with added Nb+B and T6.
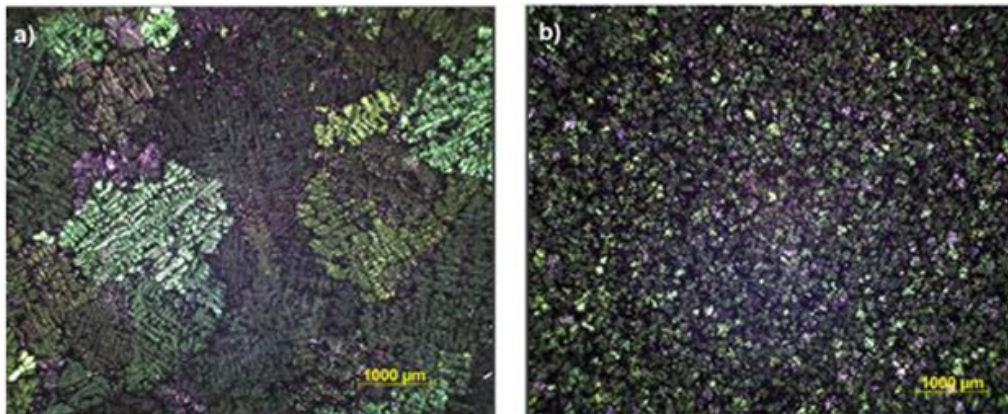
Results and Discussion

Figure 5: Primary α-Al grain size. a) without addition and b) with the inoculant NbB (0.05 Wt.% Nb).
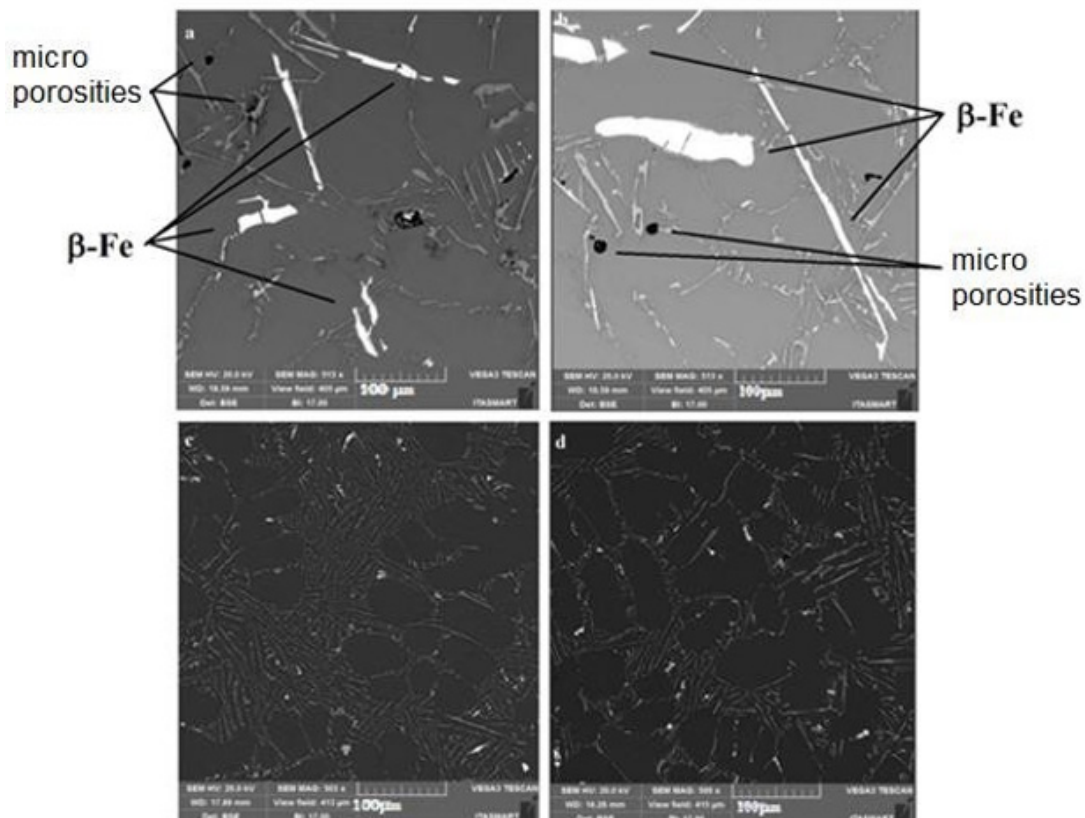

Figure 6: Image (a and b) showing the morphology of β-Fe spectra (light gray) of elongated and large shape with scattered microspores in the material structure, before the addition of Nb+B and image (c and d) showing the morphology of β-Fe spectra (light gray) of spheroidized shape and reduced size and with pore- free material structure, after the addition of Nb+B.

The reduction in average grain size was from 968μm to 221μm, compared to the base alloy without the addition of the inoculant. Figure 5 shows the size of the α-Al grains. Besides causing grain refinement, this phenomenon also creates a mechanism that modifies the morphology of the β-Fe precipitates. Figure 5 shows the difference in morphology and size of the β-Fe precipitates by SEM images. The spectra of β-Fe are highlighted by light gray color, being in the samples without addition of the inoculant of elongated and large shape, as can be seen in (Figures 6a & 6b) and in the samples with addition of the inoculant Nb+B, the precipitates of β-Fe, present spheroidized shape, and reduced size, as shown in (Figures 6c & 6d). This is a highly desirable condition of the

material structure. The analysis of (Figure 6) showed the drastic reduction in the size of the β-Fe intermetallic precipitates and practically the extinction of microporosity points in the material structure. By studying the morphology of the β-Fe particles, changes in the size of the precipitates were found, leading to reduced and scattered particles in the material structure, as can be seen in (Figures 6c & 6d). This reduction may be happening due to the evolution of liquid Al during its solidification. The solute elements (Si and Fe) are expelled from the primary α-Al grains until the concentration of the eutectic phase (12.6% by weight of Si) is reached, where the Fe particles have precipitated together with the eutectic Si. Since any solidification event takes place by nucleation and growth, it can be proposed that with nucleation at the several simultaneous points of the α-Al dendritic grains (heterogeneous nucleation), the solute rejected at the solidification front and in the eutectic pools, but now trapped between the several, reduced dendritic arms of the Al grains, end up having no approximations, clusters or interconnectivity between the partner solute elements i.e., the concentration gradient of the same element was reduced for the growth of the second phase precipitates, consequently reducing the size of the precipitated particles, which due to the more homogeneous distribution of the solute elements dispersed in the material, gave a new dynamic to the formation mechanism of the β-Fe precipitates. Also, the inoculant Nb+B addition showed a reduction in micro porosities as per (Figures 6c & 6d). The micro porosities are caused by the oxide films in the liquid metal. Theoretically, these films also act as a substrate for nucleation of β-Fe intermetallic phase formation. Therefore, without the micro porosities, it is expected that fewer β-Fe precipitates will be formed in the material.

Tensile tests were performed to study the mechanical behavior of the material on the CDPs before and after the heat treatment (T6). The results were tabulated as show in Table 2. The Al10Si1Fe alloy was taken as a reference with a Si content of 10% by weight because it is a value that favors greater strength and less damage to the ductility of the material and because it contains the critical Fe content (1% by weight), to simulate the alloys coming from recycling. The curves showed below, were built with different colors, red for the base material, blue for the base material plus the addition of Mg, purple for the base material plus addition of NbB inoculant, green for the base material with the addition of NbB, and heat treatment and the gray curve for the complete alloy, i.e., base material plus NbB inoculant, the addition of Mg and subsequent T6 heat treatment. The explanation of the results with the base material (red curve), with the material with the addition of the inoculant NbB (purple curve), highlighted in (Figure 7), can be understood due: The increase in the yield strength of the material and the strength limit can be explained due to the reduced grains with the inoculation via Nb+B, which ended up having a refined eutectic contributing to a greater dispersion of Si and also decreasing porosity, in addition to spreading between the primary and secondary dendritic arms bringing a greater amount of grain boundaries, the grain boundaries are discontinuities that hinder the movement of disagreements, improving the strength of the

material [13]. It should be noted that the α-Al grain inoculation via Nb+B caused a casting structure with not only equiaxial and reduced grain sizes but also a structure without coarse plates of β-Fe particles and no presence of micro porosities, as verified in (Figures 6c & 6d) - with Nb+B, which also contributes to the improved strength of the material [7]. Especially in hypoeutectic alloys (with Si content below 12.7%), the α phase is the continuous phase in the microstructure and is the phase determining the mechanical properties of these alloys. The β-phase is mainly formed by silicon and second phase precipitates, such as β-Fe. Since the mechanical properties of the alloy arise from the mixture between these phases, i.e., in dendrite regions, the mechanical properties are similar to those of the α phase. In contrast, in eutectic regions, the α phase is the continuous phase but intercut by the β phase. The presence of the β phase distributed over the α phase matrix raises the hardness, yield strength, and tensile strength of the alloys but drastically reduces the ductility [14]. On the fractured face of the CDP, it was observed that the rupture shows aspects of a brittle material [15], as per Figure 8. It is suggesting that the smaller grains made the material stiffer. It is signaling that only the addition of the inoculant Nb+B was not enough to achieve the mechanical properties of elongation desired to the material with Fe-critical. The explanation of the results with the base material (red curve), with the material with the addition of the inoculant NbB and T6 (purple curve), highlighted in (Figure 9), can be understood due: It is known that the production of parts with high ductility requires obtaining microstructures without the presence of elongated second phase particles and micro porosities [14], as is the case of CDPs inoculated via Nb+B (green curve under analysis), with the main second phase particles reduced and spheroidized, with this improved ductility. Similar results were also found in the work of [7]. With this, plastic deformation started at a lower strain plateau but extended to about 7.6% strain. Although the precipitation treatment was performed on the CDPs, it did not promote the hardening effect, with the formation of precipitates consistent with the α-phase matrix (precipitate maintains the crystalline lattice of the matrix), this is because there is no precipitating element in the alloy that allows the precipitation of finely dispersed particles from the supersaturated solid solution. There was a greater tendency for grain growth with the high temperature and long treatment time [16]. With this, the material behavior remained similar to the base material concerning the strength limit. During the grain refinement and solubilization treatment, the silicon and iron particles change their morphologies. Initially, continuous particles undergo a process of fragmentation and rounding (spheroidization) of the individual particles [14]. This was confirmed in this research, as shown in Figure 10, where an example of the evolution in the morphology of the β-Fe precipitates found in the samples analyzed in the various conditions studied is shown: (Figure 10a) Al10Si1Fe alloy, β-Fe precipitates in primitive form, in (Figure 10b) Al10Si1Fe0.35Mg+(T6), deformed β-Fe precipitates after heat treatment; and (Figure 10c), Al10Si1Fe0.35Mg+NbB+T6, with spheroidized Fe precipitates after grain refinement and heat treatment.

Table 2: Shows the results achieved for the five types of specimens tested.

Alloy Condition: Composition and Heat Treatment	Yield Strength (MPa)	Ultimate Tensile Strength (MPa)	Elongation (%)
Base material - Al10Si1Fe	96±2	197±3	2,1±0,1
Al10Si1Fe0,35Mg T6	143±3	191±4	3,6±0,1
Al10Si1Fe0,05Nb0,0063B	215±3	268±5	1,8±0,1
Al10Si1Fe0,05Nb0,0063B T6	78±7	194±8	7,6±0,2
Al10Si1Fe0,05Nb0,0063B0,35Mg T6	208±6	300±7	4,7±0,1
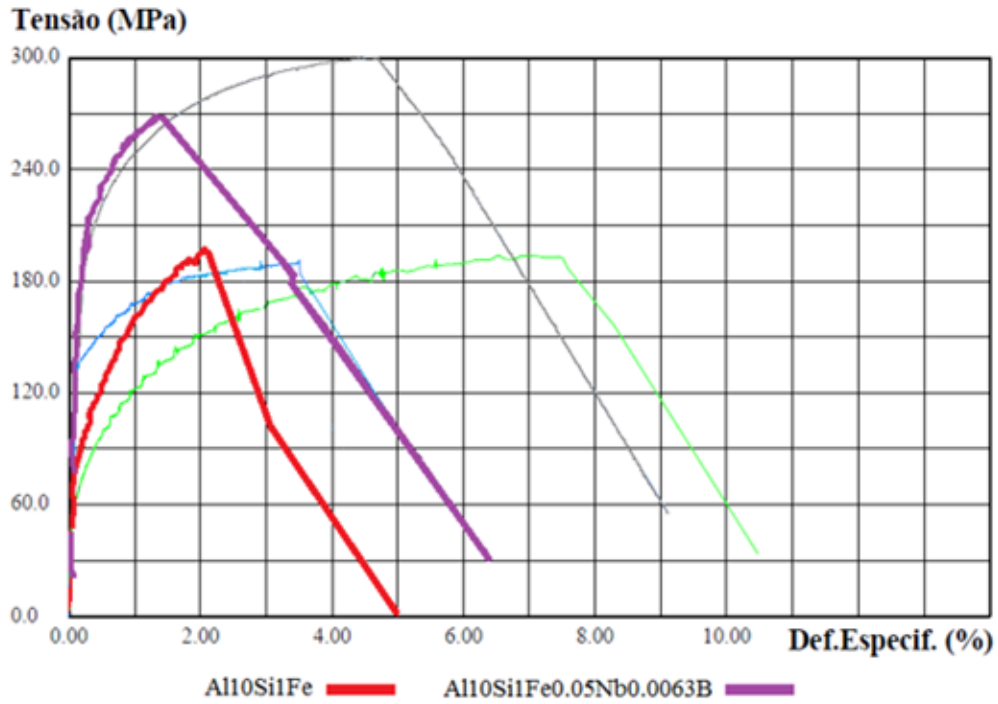
Figure 7: StressxDeformation Graph for cast CDPs. Base material (red curve); with the addition of Nb+B (purple curve).
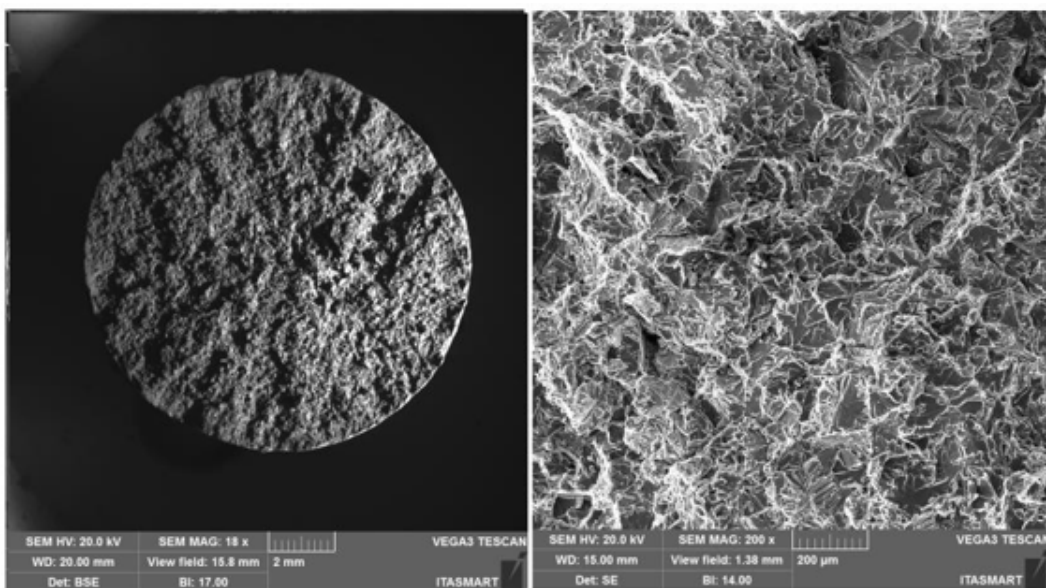

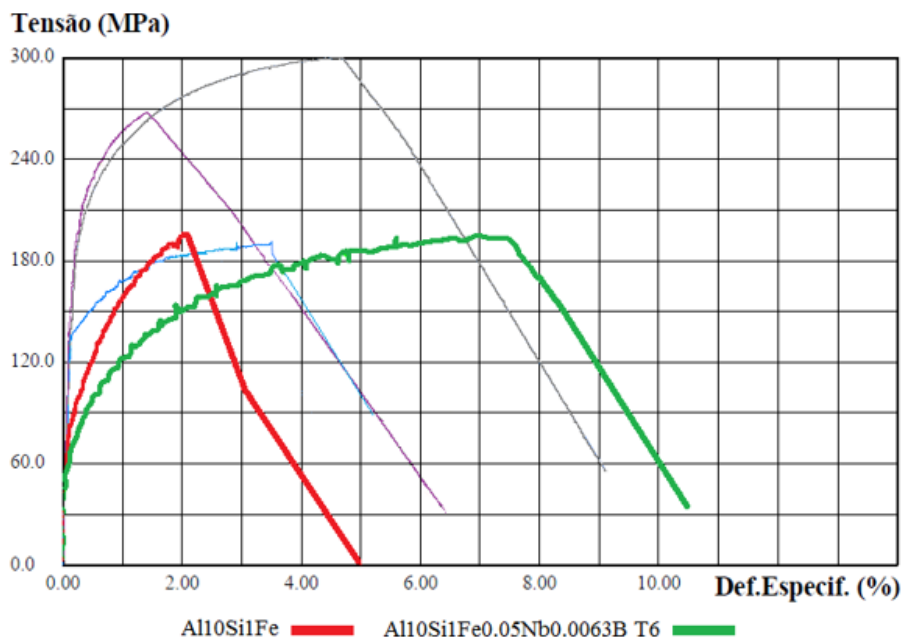**Figure 8:** Fractured face of the CDP, sample Al10Si1Fe0.05Nb0.0063B.

Figure 9: StressxDeformation Graph for cast CDPs. Base material (red curve); with the addition of Nb+B and T6 (green curve).
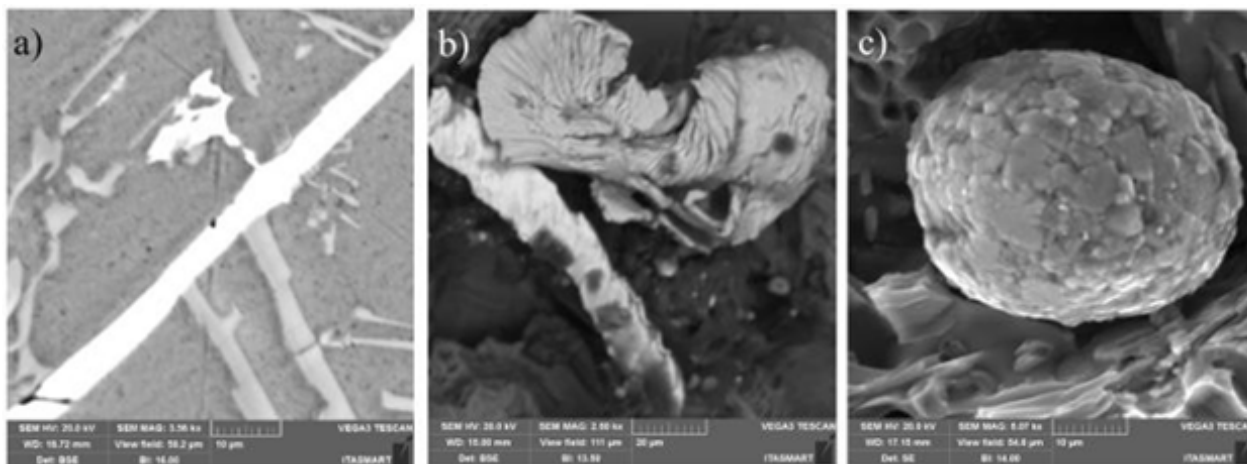

Figure 10: Fe precipitated particle evolution. (a) Al10Si1Fe alloy, β-Fe precipitates in primitive form. (b) Al10Si1Fe0.35Mg + (T6) deformed β-Fe precipitates after heat treatment. (c) Al10Si1Fe0.35Mg+NbB+T6, with spheroidized Fe precipitates after grain refinement and heat treatment.

The explanation of the results with the base material (red curve), with the material with the addition of the element Mg and T6 (blue curve), highlighted in (Figure 11), can be understood due: This is explained by the presence of the β-Fe particles coming from the Fe-critical in the base material, with a coarse plate- or needle-shaped morphology, as shown in (Figures 6a & 6b) - without the addition of Nb+B, the arrangement of the ß Al5FeSi compounds tends to form cavities in which micropores are found. With this, Fe-rich beta-phases significantly influence local stress concentrations and thus crack initiation that ultimately impacts the strength limit of the material [1,6]. After the solubilization and precipitation heat treatment, the β-Fe particles are found with distorted and decomposed morphology, as observed in Figure

12. The decomposed shape indicates the dissolution process that these phases underwent, thus obtaining a more ductile fracture mode with an increase in elongation [6]. On the other hand, the Mg$_2$Si precipitate, formed with the addition of the Mg element in the alloy and subsequent T6 heat treatment, forms solubilized and precipitated finely dispersed particles [15], serving as a reinforcement mechanism for the material in its elastic region, which justifies the increased yield strength found. However, when the deformation of the material enters the plastic region, with the increase in stress, the β-Fe particles, although deformed, are still weak points in the structure of the material. One should also observe the microporosities arising from the Fe-criticality in the alloy [6]. With this, the possibility of these regions initiated the

cracks, which eventually embrittle and limit the maximum strength of the material [2,6]. Signaling that the heat treatment (T6) has no beneficial effect on the strength limit (UTS) in alloys with Fe-critical. The explanation of the results with the base material (red curve), with the material with the addition of Nb+B, the Mg element and T6 (gray curve), highlighted in (Figure 13), can be understood due: The refinement promoted by adding the inoculant Nb+B did not alter the precipitation hardening mechanism of Mg_2Si. Likewise,

the solubilization of the material did not harm the morphology of the reduced and spheroidized β-Fe particles. The beneficial actions of the two techniques added up, providing strength and ductility to the material. The best combination of properties was observed with the addition of the inoculant via Nb+B and incorporated to the alloy the element Mg with the aging treatment (T6). It suggested the possibility of using alloys coming from recycling (Fe-critical) to produce structural and safety parts.
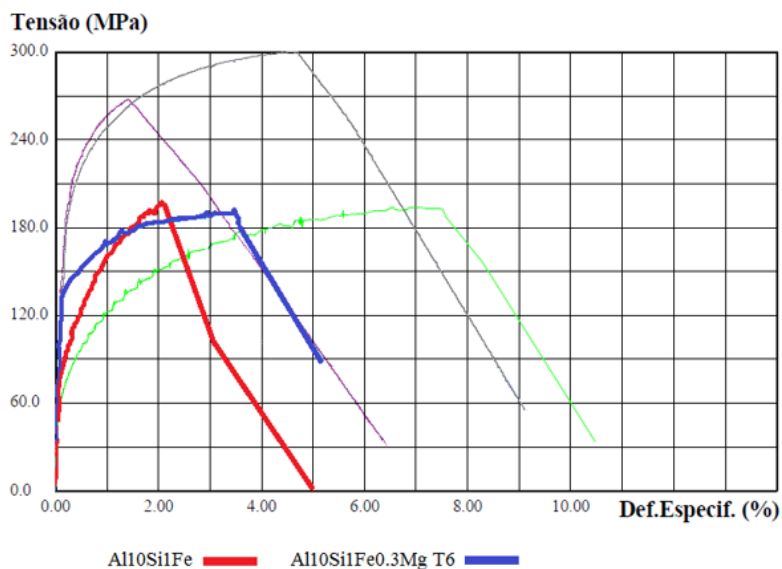

Figure 11: StressxDeformation Graph for cast CDPs. Base material (red curve); with the addition of the Mg element and T6 (blue curve).
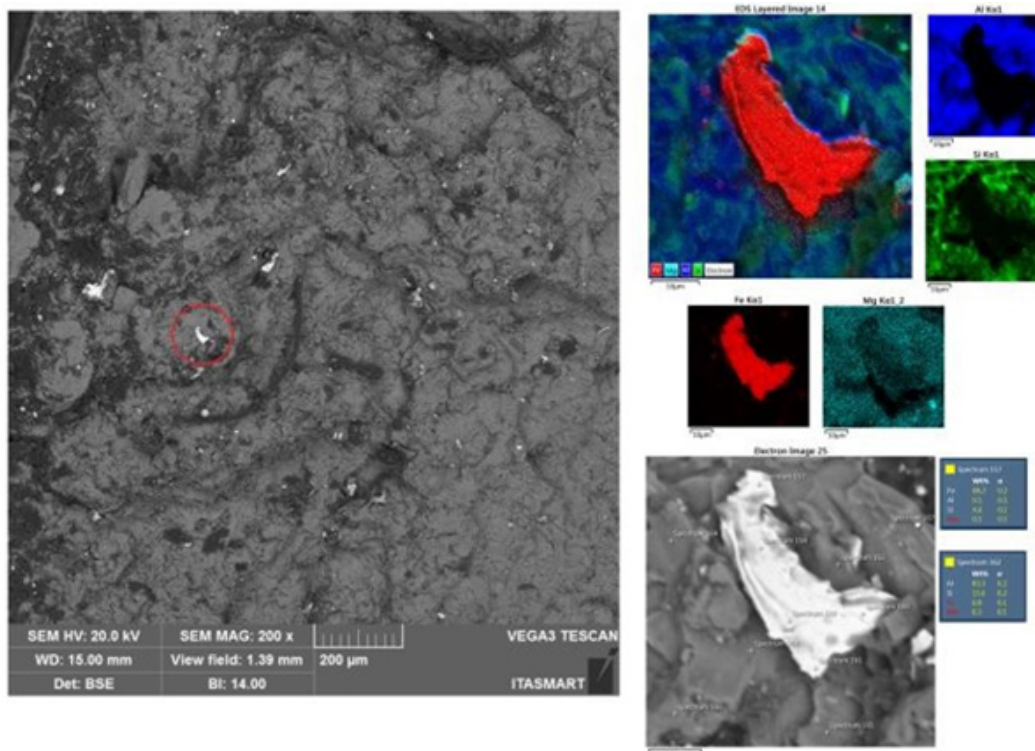

Figure 12: SEM-EDS showing the morphology of the deformed β-Fe precipitates after solubilization and precipitation treatment, found on the surface of the fractured CDP face of Al10Si1Fe0.35Mg T6 alloy.
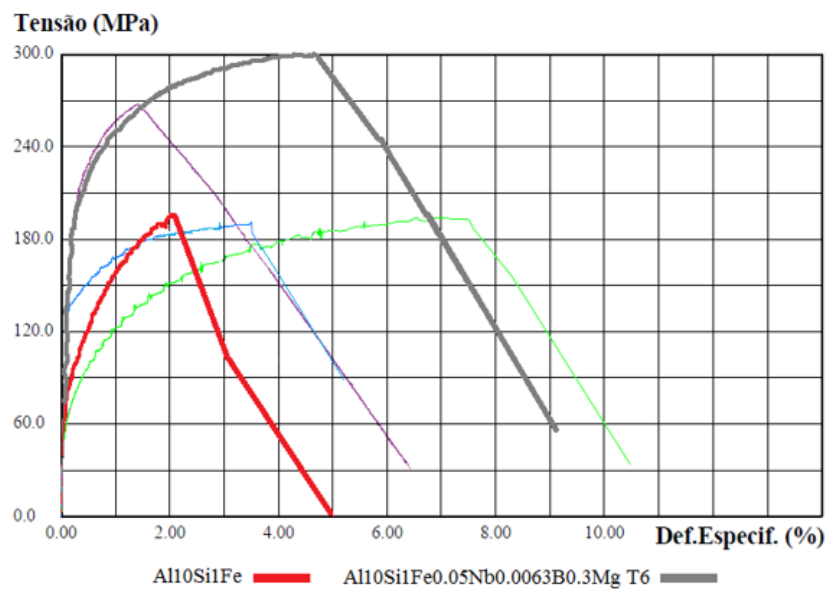
Figure 13: StressxDeformation Graph for cast CDPs. Base material (red curve); with the addition of Nb+B, the Mg element and T6 (gray curve).

Conclusion

During solidification, the solute elements (Si and Fe) are expelled from the primary α-Al grains until the concentration of the eutectic phase is reached, where the Fe particles have precipitated together with the eutectic Si. With nucleation at the several simultaneous points of the α-Al dendritic grains, the solute rejected at the solidification front and in the eutectic pools, but now trapped between the several and reduced dendritic arms of the Al grains, eventually reduce the concentration gradient of the same element for the growth of the second phase precipitates, consequently reducing the size of the precipitated particles, which gave a new dynamic to the formation mechanism of the β-Fe precipitates. With this, the condition that presented the best results in tensile properties was with the Al10Si1Fe cast alloy, inoculated with 0.05% Nb and 0.063% B, with the introduction of the Mg element and performance the precipitation aging heat treatment (T6). Thus confirming the hypothesis:

$$\sum NbB + Mg + T6 \Rightarrow \{(<\beta\text{-Fe}) \text{ A } (Mg_2Si)\} \mid \text{gain } (> \text{strength}) \text{ A } (> \text{ductility}) \text{ in the material.}$$

Acknowledgment

References

1. Taylor JA (2012) Iron-containing intermetallic phases in Al-Si based casting Alloys. Procedia Materials Science 1: 19-33.

2. Mahta M, Emamy M, Cao X, Campbell J (2007) Overview of α-Al5FeSi phase in Al-Si alloys. Materials Science Research Trends, Nova Science Publishers, USA.

3. Ebhota WS, Jen TC (2018) Intermetallic formation and their effect on mechanical properties of Al-Si-X Alloys. USA

4. Basak CB, Babu NH (2016) Morphological changes and segregation of β-Al₉Fe₂Si₂ phase: A perspective from better recyclability of cast Al-Si alloys. Materials and Design 108: 277-288.

5. Easton M, John D (2005) An analysis of the relationship between grain size, solute content, and the potency and number density of nucleant particles. Metall Trans A 36: 1911-1920.

6. Bacaicoa I, Luetje M, Wicke M, Geisert A, Zeismann F, et al. (2016) 3D morphology of Al₅FeSi inclusions in high Fe-content Al-Si-Cu Alloys. Structural Integrity Procedia 2: 2269-2276.

7. Nowak M, Bolzoni L, Babu NH (2015) Grain refinement of Al-Si alloys by Nb-B inoculation. Part I: Concept development and effect on binary alloys. Materials & Design 66: 366-375.

8. Bolzonia L, Babu NH (2016) Engineering the heterogeneous nuclei in Al-Si alloys for solidification control. Applied Materials Today 5: 255-259.

9. Li Y, Jiang Y, Liu B, Luo Q, Hu B, et al. (2021) Understanding grain refining and anti Si-poisoning effect in Al-10Si/Al-5Nb-B system. Journal of Materials Science & Technology 65: 190-201.

10. Narducci CJ, Brollo GL, Siqueira RHM, Antunes AS, Abdalla AJ (2021) Effect of Nb addition on the size and morphology of the β-Fe precipitates in recycled Al-Si alloys. Scientific Reports.

11. Narducci CJ, Antunes AS, Abdalla AJ (2021) Effect of the heterogeneous nucleation of the primary α-Al grain via the Al-4Nb-0.5B master alloy in Al-Si alloys with high Fe contents. Materials Research 24(4).

12. Apelian D (2009) Aluminum cast alloys: Enabling tools for improved performance. North American Die Casting Association. USA.

13. Mcqueen JH, Spigarelli S, Kassner ME (2011) Evangelista E hot deformation and processing of aluminum alloys. CRC Press, USA.

14. Fuoco R (2017) Mechanical properties of Al-Si alloy castings. In: Congresso De Fundição, São Paulo, Brazil.

15. Callister WDJ (2005) Fundamentals of Materials Science and Engineering. (2nd edn) Rio de Janeiro, Brazil.

16. Philipson, Fernando R, Oliveira, Glauro G (2016) Heat treatment of aluminum and its alloys. Brazil.

For possible submissions Click below:

Submit Article